JOURNAL OF GEOPHYSICAL RESEARCH, VOL. 113, D03203, doi:10.1029/2007JD009042, 2008

Coatings and their enhancement of black carbon light absorption in the tropical atmosphere

J. P. Schwarz,[1,2] J. R. Spackman,[1,2] D. W. Fahey,[1,2] R. S. Gao,[1] U. Lohmann,[3] P. Stier,[4] L. A. Watts,[1,2] D. S. Thomson,[1,2] D. A. Lack,[1,2] L. Pfister,[5] M. J. Mahoney,[6] D. Baumgardner,[7] J. C. Wilson,[8] and J. M. Reeves[8]

Received 4 June 2007; revised 7 September 2007; accepted 16 November 2007; published 14 February 2008.

[1] Black carbon (BC) is the dominant aerosol absorber of solar radiation in the atmosphere and is an important component of anthropogenic climate forcing. BC's role is strongly dependent on its physical state, which can influence the way that BC particles may act as ice and cloud nuclei, as well as the way they interact with solar radiation. In situ measurements made with a single-particle soot photometer flown on a NASA high-altitude research aircraft show the mass and size of individual BC particles in the tropics, as well as their propensity to be found mixed with additional materials. Mie theory was used to connect observed light scattering off BC particles to the optical effects of coatings on the particles. The observations indicate that as BC from ground-based emission sources rises in altitude to the lower stratosphere, coatings on BC particles become both thicker and more prevalent, while BC mass mixing ratios decrease dramatically from their values near the ground. Coatings enhance light absorption by the ambient BC column by at least 30%. These results reveal the microphysical state of BC in the atmosphere while providing important constraints for models evaluating BC's role in climate change.

Citation: Schwarz, J. P., et al. (2008), Coatings and their enhancement of black carbon light absorption in the tropical atmosphere, *J. Geophys. Res.*, *113*, D03203, doi:10.1029/2007JD009042.

1. Introduction

[2] Black carbon (BC) is the refractory and most strongly light-absorbing component of soot, a nearly omnipresent by-product of inefficient combustion. Airborne BC is the most significant particulate absorber of solar radiation in the atmosphere and an important contributor to both global- and regional-scale climate forcing [*Chylek et al.*, 1984; *Ramanathan et al.*, 2001; *Jacobson*, 2004, 2006; *Koch and Hansen*, 2005; *Chung and Seinfeld*, 2005; *Tripathi et al.*, 2005]. The current estimates of BC global radiative forcing from fossil fuel and biomass burning are near 0.4 W/m^2, comparable to the contribution of methane, the second most important greenhouse gas [*Forster et al.*, 2007]. On regional scales BC forcing estimates can be much higher (>20 W/m^2) [*Tripathi et al.*, 2005; *Ramanathan et al.*, 2001]. BC light absorption has further potential consequences, such as global dimming [*Wild et al.*, 2007]. Furthermore, regulation of BC emission sources offers potentially important opportunities for short-term mitigation of anthropogenic forcing [*Bond and Sun*, 2005].

[3] The physical state and abundance of BC throughout the atmosphere are complex functions of its varied sources and the history of the air containing it. Generally, freshly emitted BC is hydrophobic and bare of any nonrefractory material (externally mixed) [*Weingartner et al.*, 1997]. Exposure in the atmosphere transforms BC to a hydrophilic state in which individual BC particles become coated (internally mixed) with additional materials, such as sulfate and organic carbon. Here the term "coated" is used in a broad sense to refer to BC associated with different materials in a single particle. Hydrophilic coatings reduce the lifetime and atmospheric loading of BC [*Stier et al.*, 2006]. The aging process can also affect the morphology of BC particles, which may be highly nonspherical upon emission but collapse into near-spheres when processed in the atmosphere [*Ramachandran and Reist*, 1995].

[4] Coatings of additional materials can dramatically change BC's role in climate forcing. Hydrophilic coatings are thought to mediate BC's effectiveness in nucleating ice and water particles and, hence, in indirectly forcing climate [*Hendricks et al.*, 2005; *Möhler et al.*, 2005]. Presently only

[1]Chemical Sciences Division, Earth System Research Laboratory, NOAA, Boulder, Colorado, USA.
[2]Also at Cooperative Institute for Research in Environmental Sciences, University of Colorado, Boulder, Colorado, USA.
[3]Institut für Atmosphäre und Klima, ETH Zurich, Zurich, Switzerland.
[4]Department of Environmental Science and Engineering, California Institute of Technology, Pasadena, California, USA.
[5]NASA Ames Research Center, Moffett Field, California, USA.
[6]Jet Propulsion Laboratory, California Institute of Technology, Pasadena, California, USA.
[7]Centro de Ciencias de la Atmósfera, Universidad Nacional Autónoma de México, Mexico City, Mexico.
[8]Department of Engineering, University of Denver, Denver, Colorado, USA.

0148-0227/08/2007JD009042$09.00

very limited information about the nucleation efficiency of ambient BC is available. Optically significant coatings can enhance the absorption of solar radiation by BC aerosol [*Jacobson*, 2006; *Lesins et al.*, 2002; *Schnaiter et al.*, 2005; *Mikhailov et al.*, 2006; *Bond et al.*, 2006], perhaps by a factor 2, thereby increasing its direct climate forcing. A great deal of uncertainty is associated with enhanced absorption because of the difficulty in modeling the optical properties of morphologically complex aerosols and the paucity of direct measurements constraining BC mixing state in the atmosphere. The effects of coatings on the optical properties of BC have been addressed primarily in theoretical treatments [*Jacobson*, 2006; *Lesins et al.*, 2002; *Bond et al.*, 2006] and in the laboratory [*Schnaiter et al.*, 2005; *Mikhailov et al.*, 2006]. Absorption enhancement introduces an important ambiguity in relating BC mass loadings to BC absorption, which can cause systematic errors in modeling BC radiative effects and in interpreting measurements of ambient BC concentrations that are based on absorption measurements [e.g., *Sato et al.*, 2003]. To correctly model enhanced absorption, the size distributions of BC cores and their associated coatings must be known [*Bond et al.*, 2006].

[5] Here we present in situ single-particle measurements of BC-containing aerosols in cloud-free air throughout the troposphere and into the lower stratosphere over Costa Rica during the tropical winter, 2006. The BC measurements were made with a single-particle soot photometer (Droplet Measurement Technologies, Boulder, Colorado) [*Schwarz et al.*, 2006; *Slowik et al.*, 2007; *Gao et al.*, 2007] that uses four optical detectors to record the interaction of individual particles with an intense infrared intracavity laser beam. The photometer uniquely examines atmospheric BC-containing particles in the fine mode by providing a measurement of their refractory carbon masses. In this study the photometer capabilities have been expanded to allow detection of coating material associated with individual BC particles and measurement of the particles' unperturbed optical sizes. A Mie theory shell-and-core model is used to extend the optical size and carbon mass measurements to the thickness of coating material and the resulting enhancement of the absorption associated with a BC particle. In the material presented here, we (1) describe the experimental approach used, (2) explain the theory used to connect observed quantities to the optical properties of BC, (3) present measurements and analysis resolved by altitude with comparison to model results, and (4) discuss the implications of these results for global- and regional-scale modeling of atmospheric BC.

2. Experimental and Analytical Techniques

2.1. Detection of Black Carbon Aerosol

2.1.1. Sampling of Ambient Aerosol

[6] In situ measurements of BC and total aerosol were made with the photometer aboard the NASA WB-57F high-altitude research aircraft operating from San Jose, Costa Rica (10°N, 84°W) between 10°N and 1°S latitude and up to 19.4 km altitude. Total aerosol above 8 km was concurrently measured using the Focused Cavity Aerosol Spectrometer (FCAS) [*Jonsson et al.*, 1995], which provides total aerosol size distributions in the size range of 100–3000 nm. Passive near-isokinetic external inlets were used by both instruments to sample ambient air [*Jonsson et al.*, 1995; *Schwarz et al.*, 2006]. The identical inlets were designed to allow real-time measurements of deviations from isokinetic conditions. In the photometer the biases in measured particle concentrations due to the observed deviations are small; for 800-nm particles with density 1.5 g cm^{-3} the bias is less than 10% at ambient pressures greater than 150 hPa and less than 5% at higher altitudes. These values bound the possible biases of smaller particles. Transport losses in the sample lines from the inlet to the photometer were measured in the laboratory and are negligible [*Schwarz et al.*, 2006].

[7] In the present study only cloud-free air was analyzed because large ice and water particles generate artifact particles when striking a sampling inlet [*Murphy et al.*, 2004]. Air containing large particles was identified along the flight track using measurements from the Cloud Aerosol and Precipitation Spectrometer (CAPS) [*Baumgardner et al.*, 2002].

[8] The process of bringing ambient particles into the aircraft and heating them to the operating temperature of the photometer (25°C) dries them, reducing their masses and increasing their indices of refraction. This simplifies our analysis, because the likely range of index of refraction of dry coatings is smaller than that of ambient coatings. The aerosols sampled above 5-km altitude are considered dry because the relative humidity of the sampled air is reduced to below 5% during sampling and transport to the instrument. Aerosols sampled below 5-km altitude were also considered to be dry because ambient relative humidity was quite low, averaging 53%, and ambient temperatures were always lower than the operating temperature of the photometer. The implications of measuring aerosols in dry conditions for the results presented in section 3 are discussed in section 2.2.3.

2.1.2. Measurement of BC and Fine-Mode Aerosol Mass

[9] BC-containing particles are identified by the photometer when their refractory carbon masses are heated to their boiling points (roughly 4000 K) in the laser beam [*Schwarz et al.*, 2006]. The hot BC particles incandesce, emitting detectable amounts of visible and near-visible thermal radiation. The thermal radiation temperature, as measured using two wavelength bands, is used to identify BC composition [*Schwarz et al.*, 2006]. During atmospheric sampling, essentially all ambient particles that emit thermal radiation detectable by the photometer are determined to contain BC.

[10] The peak intensity of thermal radiation from a particle is linearly proportional to its refractory carbon mass and is independent of particle morphology and mixing state [*Slowik et al.*, 2007; *Moteki and Kondo*, 2007]. The linear response of the photometer to BC mass has been demonstrated in an intercomparison with other techniques sampling flame-generated soot [*Slowik et al.*, 2007] and by calibration with spherical carbon particles over the mass range 2–100 fg (~100–600 nm volume-equivalent diameter (VED), based on an assumed density of 2 g cm^{-3}). The statistical uncertainty associated with a mass determination on a single BC particle is 30%. Mass calibrations made with spherical carbon particles (Glassy Carbon Spherical Powder

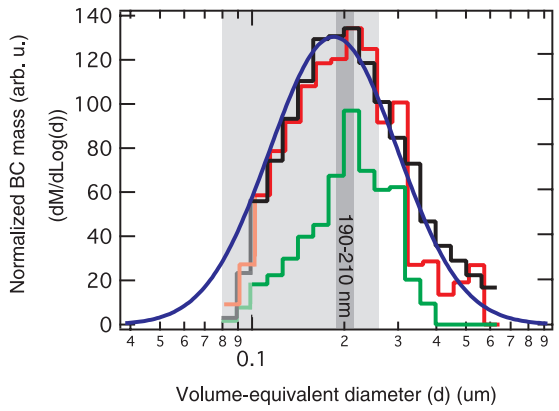

Figure 1. Fine-mode size distributions of BC mass (M) sampled on three aircraft flights over Costa Rica (1°S–10°N, 80–85°W) during 6–9 February 2006. The BC mass of all detected particles is shown in intervals of volume-equivalent diameter (d) (assuming 2 g cm^{-3} density), normalized by the total mass sampled. Two distributions are shown: all particles sampled in the range 1–5 km (black line, 31800 particles sampled) and stratospheric particles sampled in the range 17.5–19.5 km (red line, 1650 particles). Stratospheric air parcels are defined by measured ozone values above 150 ppbv. Also shown are (1) a lognormal fit to all BC larger than 100 nm diameter (blue line), (2) the distribution of sampled stratospheric particles that are associated with optical size values (green line, normalized by same factor as the stratospheric distribution), (3) the size interval for BC particles over which the mixing state was determined (100–250 nm, light shading), and (4) the range of particle sizes used in the determination of the nonrefractory-to-refractory mass ratio and coating thickness probabilities (190–210 nm, dark shading).

38004, Alpha Aesar, Inc., Ward Hill, MA, USA, and Glassy Carbon spheres, Tokai Carbon Co., LTD, Tokyo, Japan) size selected with a differential mobility analyzer were stable to better than 5% over the 4 d of measurements described in the paper.

[11] The photometer detection range for refractory carbon is ~100–600 nm VED, assuming a density of 2 g cm^{-3}. Particles having BC content within this equivalent size range are considered part of the fine mode of BC aerosol (Figure 1). The term "fine-mode" as used here is considered interchangeable with the term "accumulation-mode," as used in the literature [e.g., *Vignati et al.*, 2004]. Fine-mode BC-containing particles have a BC core in the approximate 100–1000 nm VED range.

[12] The fine mode is generally assumed to contain most of the BC mass in regions removed from BC emission sources [*Clarke et al.*, 2004; *Pöschl*, 2003]. In the UT/LS, the total aerosol mass is also dominated by the fine mode. The photometer detects 90% of the BC mass in this mode on the basis of lognormal fits to the distributions (Figure 1). Since the remaining 10% is outside the detection range of the instrument, the measured mass loadings of detected BC particles are adjusted by a factor 1.1 to account for this undetected fine-mode BC mass. Approximately 50% of the number of BC-containing particles associated with this mode is detected (not shown). An estimate of the total number concentration of BC-containing particles in the fine mode in the UT/LS is used in section 3.2. This is estimated by integrating the BC fine-mode number distribution implied by the mass distribution fits in Figure 1.

[13] Total aerosol in the fine mode in the upper troposphere and lower stratosphere was measured with the FCAS instrument. Because total aerosol mass is dominated by fine-mode contributions in this altitude range, the aerosol mass measured by the FCAS over 100–3000 nm is a good proxy for the total fine-mode mass loading. Likewise, we assume that the total number concentration of particles detected by the FCAS represents total fine-mode number concentrations.

2.1.3. Determination of BC Optical Size

[14] Non-BC particles are also detected by the photometer and are optically sized on the basis of the peak intensity of the light they scatter out of the laser beam. The peak scattering amplitude from such a particle is associated with the diameter of a dry sulfate particle that would scatter the same amount of light. The laser beam has a Gaussian intensity profile with a peak intensity that is calibrated with measurements of polystyrene latex spheres of known size before and after each flight. The peak amplitude from a single non-BC particle is uncertain to approximately 20% because all particles do not pass precisely through the center of the laser beam.

[15] Laser heating a BC-containing particle removes any coating and ultimately vaporizes the BC core. Thus the light scattered after the particle has been heated significantly is, in general, not representative of the unperturbed particle. BC particle optical size is, therefore, determined by extrapolating the light-scattering signal from a particle before it is significantly heated to its value at the center of the laser beam. Such sizing requires knowledge of the spatial profile of laser beam intensity and the position of the particle within the laser beam at every moment that it scatters light. The latter requirement is satisfied by the use of an optical detector sensitive to particle position [*Gao et al.*, 2007]. In the work presented here, the scattering signal is used only before the particles are exposed to more than 5% of the peak laser intensity. As a consequence of this extrapolation, the detection range for optical sizing is such that small BC cores (i.e., <160 nm VED) are only optically sized when they have a substantive coating. At the same time, because of detector saturation, some larger BC cores with or without coatings are too large to size optically. The detection range is ~250–450 nm in optical size.

[16] This extrapolation sizing method increases the uncertainty of the peak scattering amplitude of an individual particle by 50%, equivalent to ~11% in optical size. However, because this uncertainty is random it does not systematically shift our size results. A systematic underestimation or overestimation of the extrapolated scattering amplitude of 20% would lead only to a ±6-nm shift in average coating thickness (discussed later in this manuscript). Such a systematic uncertainty would not significantly affect the results presented here.

[17] Figure 2 shows the correlation between the scattering amplitudes of non-BC particles obtained with a full Gaussian fit and with the extrapolation method. This compact linear correlation using data collected during one flight at altitudes above 12 km demonstrate the validity of the

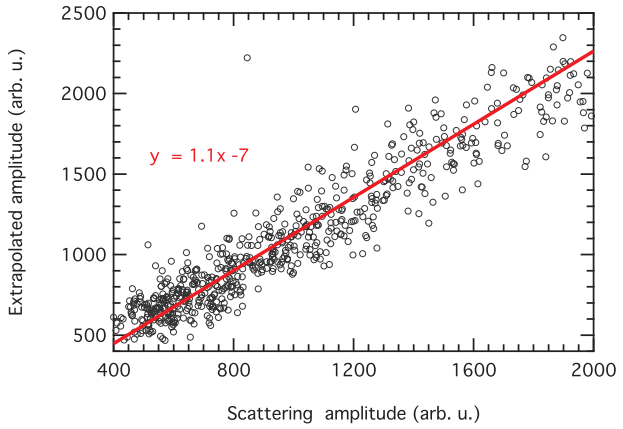

Figure 2. Correlation plot of scattering amplitudes measured for non-BC particles sampled in the lower stratosphere. The scattering amplitude on the *x* axis is obtained from a full-Gaussian fit to the scattered light signal, and the *y* axis is the amplitude extrapolated from the light scattered at the edge of the laser beam, with a maximum light intensity of 4% of the intensity at the center of the laser. The slope of the linear fit is unimportant.

extrapolation method and the working stability of the photometer. Figure 3 is a summary graph of BC particle optical size determinations, showing that increasingly large BC cores are associated with increasing optical size. It also shows that the number of BC particles detected decreases with core size. In addition, there is a range of optical size associated with any given BC core size due to the presence of different amounts of coating material on individual particles. These basic dependencies are expected for particles in the fine mode.

2.1.4. Distinguishing Bare From Coated BC

[18] A coated BC particle is distinguished from bare refractory carbon material by analysis of the laser light scattered from the particle as the laser heats it. The primary method for identifying coated (or internally mixed) BC particles is based on recognizing any clear reduction in the scattering signal measured for a BC particle occurring more than 0.4 μs before the refractory particle reaches its vaporization temperature (onset of incandescence). The reduction in scattering signal is a sign that nonrefractory material has been vaporized through heating the BC component [*Gao et al.*, 2007; *Moteki and Kondo*, 2007]. Generally, more than 95% of BC particles determined to have a coating are identified this way. Morphological changes in a BC particle as it is heated, but before it begins to vaporize, are not believed to result in significant changes in the scatter signal. The fact that many BC particles are identified as bare supports this assumption, as does the fact that the extrapolated scattering amplitudes of BC cores at full incandescence are within a factor of two of those of bare BC. This approach to determining coating state is more direct than that used in our previous study in which the correlation between the time delays between the peak scattering to peak incandescence signals, and the ratios of these signals was used qualitatively to estimate coating state [*Schwarz et al.*, 2006].

[19] The remaining 5% of coated BC particles are identified in one of two ways. First, a scattering signal observed to persist beyond the end of BC incandescence is assumed to represent a non-BC fragment of the original particle. Second, a theoretical scattered light signal is calculated on the basis of the amount of light scattered by the fully incandescent BC core, which is assumed at that point to be bare. If the integral of this theoretical signal, up to the point of incandescence, is significantly smaller than the time integral of the observed scattered light signal, then a coating is assumed to have been present. The mixing state of particles with BC masses larger than ~16 fg (i.e., BC VED > 250 nm) is not determined because large particles saturate the photometer detectors before any nonrefractory material can be removed through heating.

[20] To estimate the detection limit for coatings on BC particles, the scattered light signals from coated particles are interpreted within the context of the Mie theory results discussed in section 2.2. For BC particles with a refractory mass of approximately 8 fg (~200-nm VED) and an unperturbed optical size consistent with a 37-nm coating, approximately 50% were identified as coated with the methods described above (Figure 3). The lower detection limit of coating thickness is expected to be smaller for identifying coatings on smaller BC cores because the scattering signals of smaller particles increase more rapidly with the addition of a given amount of material than signals from larger particles. This tendency is visible in Figure 3, where the 50% coating fraction is observed with only a 25-nm coating at BC core masses of ~3 fg. Because observed BC numbers are dominated by BC particles smaller than ~150-nm VED, we estimate a lower detection limit of 25-nm thickness of coating.

[21] Over the BC size range of 100–250 nm VED, the number fraction of particles found to have coatings was independent of the mass of the underlying BC core. Thus, in this study, the number fraction of coated BC particles detected over this size range is assumed to be representative of all fine-mode BC particles.

2.2. Theoretical Calculations

2.2.1. Mie Theory With a Shell-and-Core Model

[22] Mie theory is used to extend the photometer measurements of optical size and BC mass to additional parameters. In a shell-and-core approach, a BC particle is idealized as a spherical core containing the refractory carbon mass and having a uniform coating of nonabsorbing material [*Toon and Ackerman*, 1981]. Here, the complex index of refraction chosen for the core (2, 1) matches *Schnaiter et al.* [2005], while that chosen for the coating (1.5, 0) is appropriate for dry sulfate or sodium chloride. When the optical size and refractory mass of a BC particle and the optical geometry of the photometer are further specified, the calculations provide coating thickness, single-scattering albedo (SSA), and the enhanced absorption of the BC core due to the coating. The Mie calculations reproduce, within a factor of two, the scattered light intensities measured from bare atmospheric BC particles in the size range of ~200–300 nm VED (Figure 3). This level of agreement is surprising since there is no strong physical basis to expect, a priori, that Mie theory would correctly model fresh fractal soot behavior. The work of *Schnaiter et al.* [2005] has shown that the Mie theory calculation for a shell-and-core configuration also reprodu-

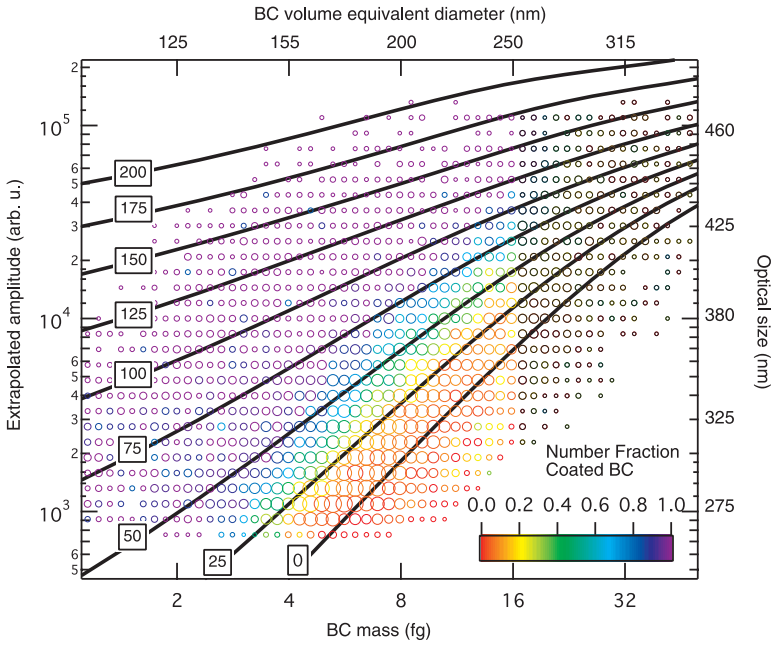

Figure 3. Summary of all observations of BC-containing particles analyzed in this study. The grid of points shows the number (area of marker) of BC particles measured in intervals of extrapolated amplitude (and optical size) and BC mass (and VED with density of 2 g cm^{-3}). The color of each circle indicates the number fraction of coated BC particles detected by the photometer. Black circles represent an undetermined number fraction. Optical size is the diameter of dry sulfate particle that would scatter the same amount of light in the photometer as the dry, but otherwise unperturbed, sampled BC particle. The scaling to optical size is based on laboratory calibrations of dioctyl sebacate aerosol scattering. Dioctyl sebacate has an index of refraction close to that of dry sulfate. Contour lines are Mie calculation results for spherical BC cores with different uniform thicknesses of coating of a nonabsorbing material with index of refraction 1.5. The boxed number on each contour indicates the coating thickness in nanometers. The maximum number of particles at a grid point is 125 and the minimum is 7.

ces observed absorption enhancements in laboratory experiments with coated, but nonspherical, diesel soot.

[23] Mie theory layer calculations were made on the basis of the shell-and-core model algorithm of *Toon and Ackerman* [1981], implemented and further developed by one of the authors (D. Lack). This algorithm generated scattered light amplitudes as a function of scattering angle from a plane wave with wavelength 1.064 μm, as well as scattering, extinction, and absorption cross sections. The light-scattering signals were integrated over the solid angles detected by the photometer, a full-angle cone of 65° directed 45° from the photometer laser beam axis. Both forward and backward scattering angles were included. The integration step size was chosen such that halving it shifted results by less than 2%. Rather than explore the range of possible values of the index of refraction of BC, two reasonable values (which, essentially, bound the value (1.95, 0.79) recommended by *Bond and Bergstrom* [2006]) were used to test the sensitivity of our models to this parameter; the sensitivity is weak, as shown by the results calculated for a range of indices (Table 1). The work of *Schkolnik et al.* [2007], on the properties of biomass burning aerosols, supports the assumption that coating materials are unlikely to absorb efficiently enough to influence this work.

[24] Calculations were made for 50 diameters of spherical cores (with density 2 g cm^{-3}) between 16 and 800 nm diameter, with coatings (shells) up to 200-nm thick divided into steps of 12.5 nm. All scattering amplitude results were scaled such that theoretical results matched calibrations with polystyrene-latex spheres. The model results were used in look-up tables that associated a measured BC core mass and extrapolated scattering amplitude with the desired parameter. Figure 3 includes the results of the Mie calculations by showing the calculated optical size contours that would be associated with cores with different sulfate coating thicknesses (in nanometers).

2.2.2. Uncertainties in the Absorption Enhancement of Fine-Mode BC

[25] The Mie theory calculations provide the enhancement in the absorption of a BC core due to the presence of a given coating. Extending this to the enhancement of the total ensemble of BC measured, however, requires some additional assumptions because coating information is incomplete (see discussion in section 2.1.3). For example, in the lower stratosphere only about 50% of the BC mass in the fine mode can be associated with an optical size value (Figure 1). To bound the range of enhancement values associated with coatings on detected BC particles without optical size information, we make two limiting assumptions: First, as a lower bound, particles for which there is no optical size information are assumed to be bare, with no enhancement of absorption. Second, as an upper bound on the effect of coatings, particles with small BC mass ($\leq$210-nm VED) are assigned the largest coating that would

Table 1. Absorption Enhancement and Single-Scattering Albedo (SSA)[a]

Core Complex Index	Coating Real Index	Absorption Enhancement (1–5 km)	Absorption Enhancement (O_3 > 150 ppbv)	SSA (Bare BC) LT(LS)	SSA (Coated BC) LT(LS)
2, 1	1.4	1.30 ± 0.1	1.44 ± 0.08	0.20(0.25)	0.35(0.56)
2, 1	1.5	1.31 ± 0.1	1.50 ± 0.08	0.20(0.24)	0.35(0.57)
2, 1	1.6	1.32 ± 0.1	1.54 ± 0.09	0.20(0.25)	0.35(0.55)
1.9, 0.8	1.4	1.31 ± 0.1	1.41 ± 0.08	0.21(0.28)	0.38(0.60)
1.9, 0.8	1.5	1.32 ± 0.1	1.47 ± 0.08	0.22(0.28)	0.38(0.58)
1.9, 0.8	1.6	1.32 ± 0.1	1.50 ± 0.09	0.21(0.27)	0.38(0.59)

[a]Results for BC-containing particles detected on three tropical flights (same data set as used in Figure 1). Values for different combinations of core and coating indices of refraction are shown for 1064 nm light. Calculated values for 550 nm light are in good agreement with 1064-nm values. The absorption enhancement values represent the average of the upper and lower bound results with the uncertainty covering their range. The SSA values are for BC particles with a core size of 190–210 nm VED. In this range, 93% of the 2040 BC particles detected in the lower troposphere (LT, 1–5 km) have measured optical sizes, while in the lower stratosphere (LS, defined as having measured O_3 concentrations above 150 ppbv) only 50 particles are available with optical size values, of which 8 were identified as bare (externally mixed).

still allow the particle to be smaller than the minimum size for optical sizing, while larger BC (cores >210-nm VED) are assigned the largest coating commonly observed for ambient particles, 200 nm. The resulting upper and lower bounds are not widely separated (Table 1) because the absorption of large BC particles is not strongly influenced even by thick coatings, and the photometer tightly constrains the coating thicknesses of small particles (Figure 3). The net uncertainties associated with the results shown in Table 2 are the root-squared sum of the range of value due to coating state assumptions (i.e., ±0.1) and the range of values from index of refraction assumptions (Table 1). The effect of coatings on the undetected 10% of the BC mass in the fine-mode is not included in this estimate.

2.2.3. Effect of Drying on Coatings and Absorption Enhancement Values

[26] To relate the derived dry aerosol parameters of coating thickness and absorption enhancement to those at ambient conditions, the results of *Steele and Hamill* [1981] and *Tang* [1996] were used to estimate water vapor uptake on the particles for ambient conditions relevant to the UT/LS. Coatings were assumed to be sulfate. Water uptake on coated BC leads to a thicker coating of material with a smaller real index of refraction, which affects the enhanced absorption of the underlying BC core. The largest differences between detection and ambient conditions were found at the cold-point tropopause, which in the tropical winter has a typical temperature of 190K and a typical water vapor mixing ratio of 3 ppmv. A typical stratospheric BC particle has a 200-nm VED and a dry coating thickness of 100 nm (Table 1). Water increases the mass of the coating by a factor ~2.5 and the absorption enhancement by a factor of 1.6. In the lower tropopause, where the average coating on a BC core of the same size is only ~40 nm and ambient relative humidity is assumed to be 50%, the coating thickness roughly doubles and the enhancement is increased by a factor of 1.5, on the basis of sulfate uptake at higher temperatures from *Steele and Hamill* [1981].

2.2.4. Determination of Convective Influence

[27] The influence of convection on air sampled at a specific location along the flight track, as used in Figure 4, was evaluated in a two-step process. In the first step, 10-d diabatic back trajectories, using the Goddard Space Flight Center Trajectory Model, are calculated from each point in a cluster of 15 points surrounding the location. The cluster points span the location by ±0.3 km vertically and ±70 km horizontally in a vertical plane perpendicular to the flight track location. The cluster of points is used to evaluate trajectory errors. The second step involves running each trajectory through 3-hourly meteorological infrared (IR) satellite imagery. Convection is deemed to influence a sampling location if the cloud altitude in the imagery exceeds the trajectory altitude at one or more points along the trajectory that are geographically within 30 km of the cloud. Cloud altitude is generated by matching IR brightness temperatures with temperatures from meteorological analyses. A separation of 30 km is chosen because it is an approximate indicator of the width of anvil edges observed in convection. IR brightness temperatures are adjusted downward by about 6 K to reflect the difference between IR and lidar cloud top height measurements. The convective influence fraction for a given aircraft location is then a weighted fraction of the cluster points that are convectively influenced in the previous 10 d (with points closest to actual location of the aircraft given the greatest weight).

3. Airborne Sampling Results

3.1. Black Carbon Mass and Number

[28] The results presented here are based on three flights during the tropical dry season on 6–9 February 2006. Mass distributions of fine-mode BC cores in two altitude ranges are shown in Figure 1. The high degree of similarity between the mass distributions from the lower troposphere

Table 2. Results of Mie Theory Calculations for Ambient BC Aerosol[a]

Altitude, km	Average Coating Thickness,[b] nm	Single-Scattering Albedo[b]	Absorption Enhancement[c]
1–5	29	0.24 ± 0.1	1.31 ± 0.1
17.5–19.5	99	0.48 ± 0.2	1.50 ± 0.1

[a]The uncertainties shown are dominated by the effect of assumptions about BC particles for which no optical size (and thus no enhancement value) was available (Figure 1). The contribution of these particles is bounded by the two extremes of characterizing them as either having no coating or a thick coating. The values are only weakly dependent on assumptions of the indices of refraction of the coatings (over a range 1.4–1.6) and BC core ((1.9, 0.8)–(2, 1)) (see Table 1).

[b]For particles with a 190–210 nm VED BC core.

[c]Estimated for all BC particles in the fine mode.

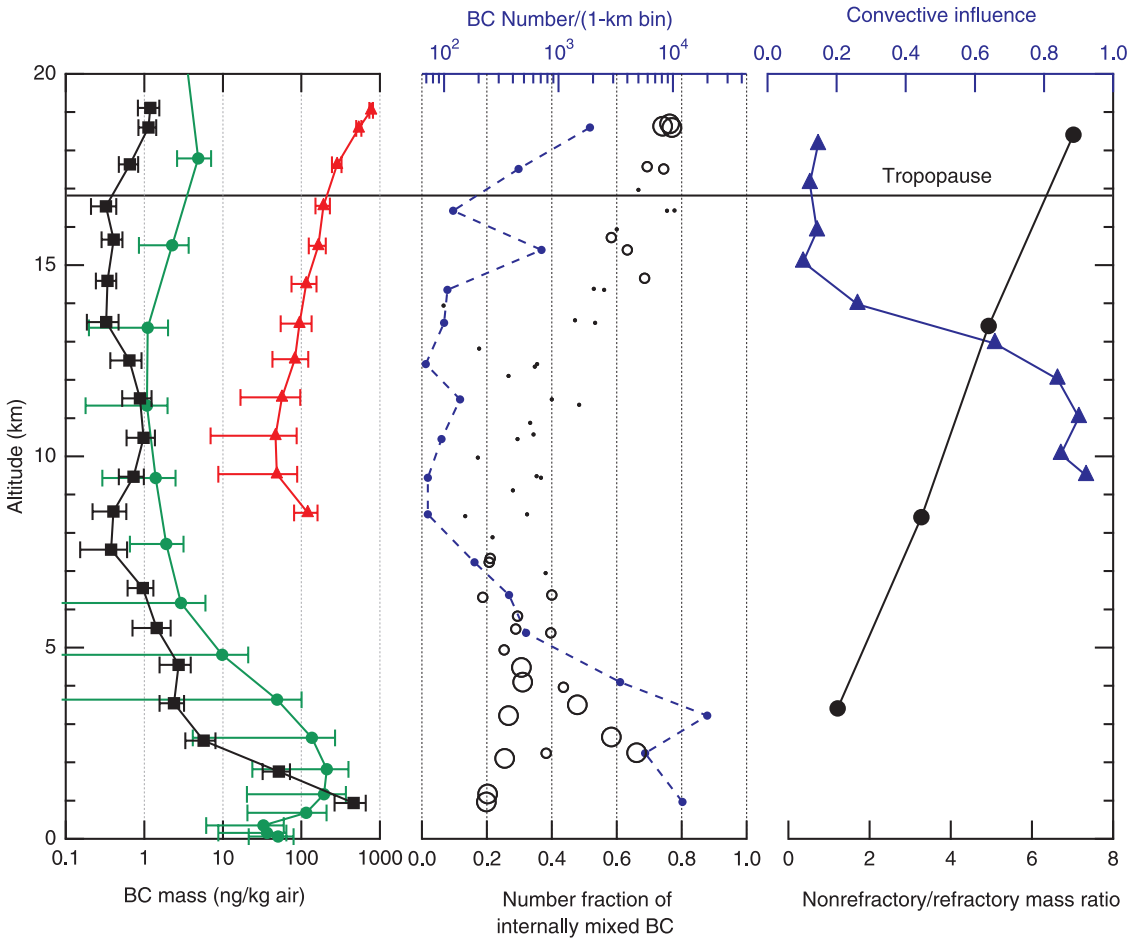

Figure 4. Vertical profile results from three Costa Rica flights (see Figure 1 caption). (left) BC mass mixing ratio (black squares) averaged over 1-km altitude intervals with total uncertainty. Mass mixing ratios of total aerosol in the size range 0.1–3 μm (red triangles) from the FCAS instrument, shown with whiskers indicating observed variability. Model results (green circles [*Lohmann et al.*, 2007]) are shown with whiskers indicating daily standard deviation. (middle) Number fraction of internally mixed BC particles (open circles) for BC cores in the range 100–250 nm VED (see Figure 1). Each symbol corresponds to a 1-km average from one flight with the symbol diameter roughly proportional to its statistical confidence; large, medium, and small symbols correspond to <5%, <10%, and $\leq$25% statistical uncertainty, respectively. The blue dashed line (top scale) shows the number of BC particles detected in each altitude interval. (right) Average ratio of nonrefractory to refractory mass associated with BC particles over the BC size range of 190–210 nm VED (see Figure 1) averaged over 5-km altitude intervals (black circles). The uncertainty associated with this ratio is 100%. Diabatic back trajectory calculations for the fraction of air influenced by convection within the 10 d preceding sampling (blue triangles, top scale). The average cold-point tropopause height is shown at 16.9 km as derived from Microwave Temperature Profiler measurements along the flight tracks [*Denning et al.*, 1989].

and stratosphere is a surprising result because it implies that the processes that create and maintain the large vertical gradients in BC mass mixing ratios are not dependent on the BC mass of removed particles. The lack of size dependence apparently conflicts with the reported importance of aerosol size on cloud nucleation efficiency [*Dusek et al.*, 2006] and, hence, may be useful in assessing the removal mechanisms used in global models.

[29] The BC mass mixing ratio shows a large vertical gradient, decreasing by about three orders of magnitude between the ground and the UT/LS (Figure 4). Surface values average 500 ng (kg-air)$^{-1}$ and UT/LS values average 1 ng (kg-air)$^{-1}$. BC mass forms roughly 1% of the dry aerosol load in the UT/LS. This small mass fraction is consistent with our observation in this data set that only ~0.7% of all high-altitude, fine-mode particles measured between 12 and 19 km contain a fine-mode BC component. Determination of this number fraction is discussed in section 2.1.2. The large vertical gradient in BC mass loadings, similar to that found in midlatitude profiles [*Schwarz et al.*, 2006], is consistent with short lifetime estimates for BC in the lower troposphere (<10 d) [*Lauer and Hendricks*, 2006]. A comprehensive global aerosol model [*Stier et al.*, 2005] coupled to a double-moment cloud microphysics scheme [*Lohmann et al.*, 2007] reproduces the character of the profile.

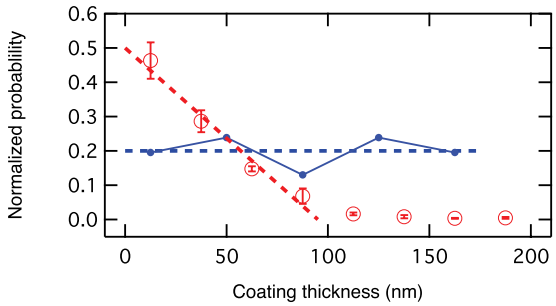

Figure 5. Normalized probability of coating thickness values detected on BC cores between 190 and 210 nm VED (see Figure 1). Information on coating thickness is most complete in this narrow size range. Red data points represent 25-nm bins averaged over 1350 particles detected between 1 and 5 km altitude, with whiskers representing statistical confidence. No estimate of statistical confidence is made for the lower stratospheric (blue line, 17.5–19.5 km) data set, which contains 46 particles and was binned over 37-nm-wide bins. Unweighted linear fits are shown for all the stratospheric data and for low-altitude values associated with thicknesses less than or equal to 100 nm (dashed lines).

3.2. Number Fraction of Coated Black Carbon Particles

[30] The number fraction of fine-mode BC particles identified as coated increases with altitude (Figure 4). Statistical confidence based on the number of BC particles sampled is greatest above 15 km and below 5 km. The variability in the low-altitude values (0.2 to 0.7) is attributable to the proximity to local BC sources, including urban emissions and biomass burning. The lowest number fractions are expected near source regions where the transformation of BC to an aged state is incomplete. In contrast, high number fractions (~0.75) with very low variability and high statistical confidence are found in the lower stratosphere. The low variability is associated with low convective influence, as calculated in section 2.2.4, with 10-d back trajectories (Figure 4). We postulate that where convective influence is low, recent surface emissions do not contribute to observed BC mass, and aging times are sufficient to allow coatings to form more completely on BC particles. In addition, greater convective influence in the middle troposphere likely contributes to the higher variability observed there. The variability at lower altitudes supports the need for high temporal and geographical resolution in regional-scale models of BC aerosol processes and subgrid-scale parameterizations in global models.

3.3. Ratio of Coating Mass to Refractory Carbon Mass

[31] The ratio of the dry coating mass to refractory carbon mass of individual BC particles shows a clear altitude dependence, with values increasing from near unity at low altitude to nearly a factor of seven in the lower stratosphere (Figure 4). This increase with altitude constrains the time constants for the accumulation of material on BC cores, and hence the transformation of BC from an externally to internally mixed state. The ratio was calculated for the BC core size range of 190–210 nm VED (Figure 1) over which the optical size measurements are most complete. For this same narrow size range, the frequency distributions of coating thicknesses in two altitude intervals (Figure 5) are consistent with the altitude dependence of coating mass. At low altitudes, the most likely coating thickness is 0–25 nm (nearly bare particles) and coating thicknesses greater than 100 nm are highly unlikely. In the stratosphere, for the few (~50) BC particles detected in this size range, all coating thicknesses in the range 12–88 nm are observed to be equally probable. These trends are also reflected in the SSA values for BC aerosol at low and high altitudes (Table 2). The low values of the SSA result from the particles' ability to absorb a great deal of light. However, as coatings accrue on a fine-mode BC particle, its scattering cross section increases more quickly than its absorption cross section, thereby increasing SSA. Very likely these trends are even larger in moist ambient conditions, as discussed in section 2.2.3.

[32] If the assumption is made that the likelihood of finding a specific coating thickness on a BC particle is independent of the underlying refractory mass for the whole fine mode, rather than only the range discussed in section 2.1.4, then the strong altitude dependence observed in the dry coating/BC mass ratio (Figure 4) is representative of all fine-mode BC. At this time, with the current performance of the photometer, the validity of this assumption cannot be assessed. However, the increase in the mass of the coatings with altitude is consistent with the increase in the internally mixed fraction and with the assertion stated above; namely, high-altitude BC aerosols have been aged over increasingly long times during which coatings are formed.

3.4. Enhancement of the Absorption of Fine-Mode BC Mass

[33] The effect of dry coatings on the absorption of fine-mode BC mass was also calculated from Mie theory (section 2.2.2). The net enhancement was found to be significantly greater than unity (Table 2) and to increase with altitude. The enhancement values place new limits on the effects of nonabsorbing material on BC's direct radiative effect. The lower tropospheric enhancement value of ~1.3 is an estimate of the enhancement of column BC absorption because BC column loading is dominated by aerosol below ~5 km (Figure 4). This value represents a lower limit on the enhancement because it is calculated for dry BC. At ambient relative humidity, coating thicknesses and associated enhancements will generally be larger, perhaps by an additional 50% (as discussed in section 2.2.3 and by *Mikhailov et al.* [2006]). These results demonstrate how the ambiguity between absorption and BC mass associated with the interpretation of absorption measurements [e.g., *Sato et al.*, 2003] is removed by detection of both refractory BC mass and coating thickness on a particle-by-particle basis. Thus emission factors and inventories can be linked more directly to observed BC mass loadings.

4. Implications for Global Models of Black Carbon Aerosol

[34] These results have important implications for models of BC aerosol. Computational constraints generally lead to approximations of BC as either being externally mixed (i.e., bare) or fully internally mixed with all other (anthropogenic)

aerosol components. Few models attempt to simulate the BC mixing state. In the ECHAM5-HAM model discussed here [*Stier et al.*, 2005], BC is emitted as an external mixture and then microphysically aged, through condensation and coagulation, to modes internally mixed with other aerosol components such as sulfate, organic carbon, sea salt, and dust. However, this common representation of the BC as uniformly mixed with other aerosol constituents contrasts with the picture developed here: while many BC particles at all altitudes may be internally mixed (Figure 4), about 99% of high-altitude fine-mode particles do not contain detectable amounts of BC. Consequently, all current global models that assume uniform internal mixing are very likely overestimating the number of fine-mode particles containing BC and overestimating the non-BC mass fraction in individual BC-containing particles by more than an order of magnitude. Aligning the representation of BC aerosol mixing state with observations is an important modeling challenge that will lead to improved estimates of solar absorption by BC and improved understanding of BC's role in nucleation of ice and water particles.

5. Conclusions

[35] A single-particle soot photometer operating on board a NASA high-altitude WB-57F research aircraft sampled tropical air from the lower troposphere to the UT/LS on 3 d of the Costa Rican dry season, February 2006. The instrument detected refractory BC cores in the size range ~100–600 nm VED, covering 90% of the mass of BC in the fine mode, and provided optical size information for a subset of dry but otherwise unperturbed BC particles. The evolution of the scattering behavior of BC particles as they were heated was used to determine whether they were coated. The refractory mass and optical size values constrained Mie theory calculations on a shell-and-core model that associated individual particles with coating thickness, single scattering albedos, and the enhancements of light absorption of the cores due to the coatings.

[36] Quantification of BC parameters revealed several robust features of BC abundance and mixing state in the tropical wintertime atmosphere. At low altitudes, where fairly new BC emissions dominate BC mass, mass mixing ratios were high (500–1000 ng/kg) while the number fraction of coated particles varied dramatically (0.2–0.7) because of the variety of contributing sources. Coating thicknesses associated with 200-nm-VED BC cores in the lower troposphere averaged ~30 nm. BC mass loadings decreased sharply from the ground to roughly 5-km altitude, falling by about a factor of 1000. The fraction of coated particles remained highly variable up to ~15 km altitude, only 2 km below the average tropical tropopause. At higher altitudes in the UT/LS, the BC mass mixing ratios showed a slight increase. In the 15–19 km region, the number fraction reached its highest and least variable values near 0.8 and a much larger average coating thickness of close to 100 nm is associated with 200-nm-VED BC cores. Although the nonrefractory mass associated with BC cores of this size increased with altitude, reaching an average of ~7 times the BC mass in the UT/LS, only ~1% of all particles in the fine mode were mixed with detectable amounts of BC above 12 km. Convective influence calculated for sampled air parcels showed the lowest values in the UT/LS where the coated fractions are highest. This correlates to altitudes where BC is expected to have been processed over long times.

[37] Coated BC particles enhance the absorption of and heating by solar radiation. The calculated enhancement is smaller in the lower troposphere than in the UT/LS. The lower-troposphere average value derived here, 1.31 ± 0.1, is appropriate for dried BC, and is considered a lower limit on the impact of coatings on the direct forcing of BC. In ambient water vapor conditions, this value could be 50% higher. These enhanced absorption values indicate that coatings on BC are important mediators of BC's role in climate change.

[38] The picture developed here of a nonuniform distribution of coating material on BC cores is generally not reproduced by contemporary global and regional aerosol models. The constraints embodied by this new description of BC's microphysical condition in the atmosphere will help direct the future development and evaluation of such models and help improve the estimation of the direct and indirect radiative forcing of BC.

[39] **Acknowledgments.** We gratefully acknowledge clarifying discussion with Johannes Hendricks, Michael Schulz, Ken Kelly, Susan Hovde, and Serena Chung. This research was supported by the NOAA Atmospheric Composition and Climate Program, the NASA Upper Atmospheric Research Program, and the NASA Radiation Science Program. Work performed by M. J. Mahoney at the Jet Propulsion Laboratory, California Institute of Technology, was done under contract with NASA.

References

Baumgardner, D., H. H. Jonsson, W. Dawson, D. O'Connor, and R. Newton (2002), The cloud, aerosol, and precipitation spectrometer (CAPS): A new instrument for cloud investigations, *Atmos. Res.*, *59–60*, 251.

Bond, T. C., and R. W. Bergstrom (2006), Light absorption by carbonaceous particles: An investigative review, *Aerosol Sci. Technol.*, *40*, 27.

Bond, T. C., and H. Sun (2005), Can reducing black carbon emissions counteract global warming?, *Environ. Sci. Technol.*, *39*, 5921.

Bond, T. C., G. Habib, and R. W. Bergstrom (2006), Limitations in the enhancement of visible light absorption due to mixing state, *J. Geophys. Res.*, *111*, D20211, doi:10.1029/2006JD007315.

Chung, S. H., and J. H. Seinfeld (2005), Climate response of direct radiative forcing of anthropogenic black carbon, *J. Geophys. Res.*, *110*, D11102, doi:10.1029/2004JD005441.

Chylek, P., V. Ramaswamy, and R. J. Cheng (1984), Effect of graphitic carbon on the albedo of clouds, *J. Atmos. Sci.*, *41*, 3076.

Clarke, A. D., et al. (2004), Size distributions and mixtures of dust and black carbon aerosol in Asian outflow: Physiochemistry and optical properties, *J. Geophys. Res.*, *109*, D15S09, doi:10.1029/2003JD004378.

Denning, R. F., S. L. Guidero, G. S. Parks, and B. L. Gary (1989), Instrument description of the Airborne Microwave Temperature Profiler, *J. Geophys. Res.*, *94*, 16,757.

Dusek, U., et al. (2006), Size matters more than chemistry for cloud-nucleating ability of aerosol particles, *Science*, *312*, 1375.

Forster, P., et al. (2007), Changes in atmospheric constituents and in radiative forcing, in *Climate Change 2007: The Physical Science Basis—Contribution of Working Group I to the Fourth Assessment Report of the Intergovernmental Panel on Climate Change*, edited by S. Solomon et al., p. 129, Cambridge Univ. Press, New York.

Gao, R. S., et al. (2007), A novel method for estimating light-scattering properties of soot aerosols using a modified single-particle soot photometer, *Aerosol Sci. Technol.*, *41*, 125.

Hendricks, J., B. Kärcher, U. Lohmann, and M. Ponater (2005), Do aircraft black carbon emissions affect cirrus clouds on the global scale?, *Geophys. Res. Lett.*, *32*, L12814, doi:10.1029/2005GL022740.

Jacobson, M. Z. (2004), Climate response of fossil fuel and biofuel soot, accounting for soot's feedback to snow and sea ice albedo and emissivity, *J. Geophys. Res.*, *109*, D21201, doi:10.1029/2004JD004945.

Jacobson, M. Z. (2006), Effects of externally-through-internally-mixed soot inclusions within clouds and precipitation on global climate, *J. Phys. Chem. A*, *110*, 6860.

Jonsson, H. H., et al. (1995), Performance of the Focused Cavity Aerosol Spectrometer for measurements in the stratosphere of particle size in the 0.06–2 micrometer diameter range, *J. Atmos. Oceanic Technol.*, *12*, 1151995.

Koch, D., and J. Hansen (2005), Distant origins of Arctic black carbon: A Goddard Institute for Space Studies ModelE experiment, *J. Geophys. Res.*, *110*, D04204, doi:10.1029/2004JD005296.

Lauer, A., and J. Hendricks (2006), Simulating aerosol microphysics with the ECHAM4/MADE GCM—Part II: Results from a first multiannual simulation of the submicrometer aerosol, *Atmos. Chem. Phys.*, *6*, 5495.

Lesins, G., P. Chylek, and U. Lohmann (2002), A study of internal and external mixing scenarios and its effect on aerosol optical properties and direct radiative forcing, *J. Geophys. Res.*, *107*(D10), 4094, doi:10.1029/2001JD000973.

Lohmann, U., P. Stier, C. Hoose, S. Ferrachat, E. Roeckner, and J. Zhang (2007), Cloud microphysics and aerosol indirect effects in the global climate model ECHAM5-HAM, *Atmos. Chem. Phys. Disc.*, *7*, 3719.

Mikhailov, E. F., S. S. Vlasenko, I. A. Podgorny, V. Ramanathan, and C. E. Corrigan (2006), Optical properties of soot–water drop agglomerates: An experimental study, *J. Geophys. Res.*, *111*, D07209, doi:10.1029/2005JD006389.

Möhler, O., et al. (2005), Effect of sulfuric acid coating on heterogeneous ice nucleation by soot aerosol particles, *J. Geophys. Res.*, *110*, D11210, doi:10.1029/2004JD005169.

Moteki, N., and Y. Kondo (2007), Effects of mixing state on black carbon measurements by laser-induced incandescence, *Aerosol Sci. Technol.*, *41*, 398.

Murphy, D. M., D. J. Cziczo, P. K. Hudson, D. S. Thomson, J. C. Wilson, T. Kojmia, and P. R. Buseck (2004), Particle generation and resuspension in aircraft inlets when flying in clouds, *Aerosol Sci. Technol.*, *38*, 400.

Pöschl, U. (2003), Aerosol particle analysis: challenges and progress, *Anal. Bioanal. Chem.*, *375*, 30.

Ramachandran, G., and P. C. Reist (1995), Characterization of morphological changes in agglomerates subject to condensation and evaporation using multiple fractal dimensions, *Aerosol Sci. Technol.*, *23*, 431.

Ramanathan, V., et al. (2001), Indian Ocean experiment: An integrated analysis of the climate forcing and effects of the great Indo-Asian haze, *J. Geophys. Res.*, *106*(D22), 28,371.

Sato, M., J. Hansen, D. Koch, A. Lacis, R. Ruedy, O. Dubovik, B. Holben, M. Chin, and T. Novakov (2003), Global atmospheric black carbon inferred from Aeronet, *Proc. Natl. Acad. Sci. U. S. A.*, *100*, 6319.

Schkolnik, G., D. Chand, A. Hoffer, M. O. Andreae, C. Erlick, E. Swietlicki, and Y. Rudich (2007), Constraining the density and complex refractive index of elemental and organic carbon in biomass burning aerosol using optical and chmical measurements, *Atmos. Environ.*, *41*, 1107.

Schnaiter, M., C. Linke, O. Möhler, K.-H. Naumann, H. Saathoff, R. Wagner, U. Schurath, and B. Wehner (2005), Absorption amplification of black carbon internally mixed with secondary organic aerosol, *J. Geophys. Res.*, *110*, D19204, doi:10.1029/2005JD006046.

Schwarz, J. P., et al. (2006), Single-particle measurements of midlatitude black carbon and light-scattering aerosols from the boundary layer to the lower stratosphere, *J. Geophys. Res.*, *111*, D16207, doi:10.1029/2006JD007076.

Slowik, J. G., et al. (2007), An intercomparison of instruments measuring black carbon content of soot particles, *Aerosol Sci. Technol.*, *41*, 295.

Steele, H. M., and P. Hamill (1981), Effects of temperature and humidity on the growth and optical properties of sulfuric acid-water droplets, *J. Aerosol Sci.*, *12*, 517.

Stier, P., et al. (2005), The aerosol-climate model ECHAM5-HAM, *Atmos. Chem. Phys.*, *5*, 1125.

Stier, P., J. H. Seinfeld, S. Kinne, J. Feichter, and O. Boucher (2006), Impact of nonabsorbing anthropogenic aerosols on clear-sky atmospheric absorption, *J. Geophys. Res.*, *111*, D18201, doi:10.1029/2006JD007147.

Tang, I. N. (1996), Chemical and size effects of hygroscopic aerosols on light scattering coefficients, *J. Geophys. Res.*, *101*, 19,245.

Toon, O. B., and T. P. Ackerman (1981), Algorithms for the calculation of scattering by stratified sphere, *Appl. Opt.*, *20*, 3657.

Tripathi, S. N., S. Dey, V. Tare, and S. K. Satheesh (2005), Aerosol black carbon radiative forcing at an industrial city in northern India, *Geophys. Res. Lett.*, *32*, L08802, doi:10.1029/2005GL022515.

Vignati, E., J. Wilson, and P. Stier (2004), M7: An efficient size-resolved aerosol microphysics module for large-scale aerosol transport models, *J. Geophys. Res.*, *109*, D22202, doi:10.1029/2003JD004485.

Weingartner, E., H. Burtscher, and H. Baltensperger (1997), Hygroscopic properties of carbon and diesel soot particles, *Atmos. Environ.*, *31*, 2311.

Wild, M., A. Ohmura, and K. Makowski (2007), Impact of global dimming and brightening on global warming, *Geophys. Res. Lett.*, *34*, L04702, doi:10.1029/2006GL028031.

D. Baumgardner, Centro de Ciencias de la Atmósfera, Universidad Nacional Autónoma de México, Ciudad Universitaria, 04510, Mexico City, Mexico.

D. W. Fahey, R. S. Gao, D. A. Lack, J. P. Schwarz, J. R. Spackman, D. S. Thomson, and L. A. Watts, Chemical Sciences Division, Earth System Research Laboratory, NOAA, Boulder, CO 80305, USA. (joshua.p.schwarz@noaa.gov)

U. Lohmann, Institut für Atmosphäre und Klima, ETH Zurich, CH-8092 Zürich, Switzerland.

M. J. Mahoney, Jet Propulsion Laboratory, California Institute of Technology, Pasadena, CA 91109, USA.

L. Pfister, NASA Ames Research Center, Moffett Field, CA 94035, USA.

J. M. Reeves and J. C. Wilson, Department of Engineering, University of Denver, Denver, CO 80208, USA.

P. Stier, Department of Environmental Science and Engineering, California Institute of Technology, Pasadena, CA 91125, USA.